Unconventional endocytosis and trafficking of transferrin receptor induced by iron

Elena Gammella[a], Irene Schiano Lomoriello[b], Alexia Conte[b], Stefano Freddi[b], Alessandra Alberghini[a], Maura Poli[c], Sara Sigismund[b,d], Gaetano Cairo[a,*], and Stefania Recalcati[a,*]

[a]Department of Biomedical Sciences for Health, University of Milan, 20133 Milan, Italy; [b]IEO, Istituto Europeo di Oncologia IRCCS, 20141 Milan, Italy; [c]Department of Molecular and Translational Medicine, University of Brescia, 25123 Brescia, Italy; [d]Department of Oncology and Hematology-Oncology, Università degli Studi di Milano, 20122, Milan, Italy

ABSTRACT **The posttranslational regulation of transferrin receptor (TfR1) is largely unknown. We investigated whether iron availability affects TfR1 endocytic cycle and protein stability in HepG2 hepatoma cells exposed to ferric ammonium citrate (FAC). NH_4Cl and bafilomycin A1, but not the proteasomal inhibitor MG132, prevented the FAC-mediated decrease in TfR1 protein levels, thus indicating lysosomal involvement. Knockdown experiments showed that TfR1 lysosomal degradation is independent of 1) endocytosis mediated by the clathrin adaptor AP2; 2) Tf, which was suggested to facilitate TfR1 internalization; 3) H-ferritin; and 4) MARCH8, previously implicated in TfR1 degradation. Notably, FAC decreased the number of TfR1 molecules at the cell surface and increased the Tf endocytic rate. Colocalization experiments confirmed that, upon FAC treatment, TfR1 was endocytosed in an AP2- and Tf-independent pathway and trafficked to the lysosome for degradation. This unconventional endocytic regulatory mechanism aimed at reducing surface TfR1 may represent an additional posttranslational control to prevent iron overload. Our results show that iron is a key regulator of the trafficking of TfR1, which has been widely used to study endocytosis, often not considering its function in iron homeostasis.**

Monitoring Editor
Patricia Bassereau
Institut Curie

Received: Feb 19, 2020
Revised: Nov 16, 2020
Accepted: Nov 19, 2020

This article was published online ahead of print in MBoC ivn Press (http://www.molbiolcell.org/cgi/doi/10.1091/mbc.E20-02-0129) on November 25, 2020.

Competing interests: No competing interests are declared.

*Address correspondence to: Gaetano Cairo (gaetano.cairo@unimi.it); Stefania Recalcati (stefania.recalcati@unimi.it).

Abbreviations used: AIRC, Associazione Italiana Ricerca sul Cancro; BAFT, bafilomycin A1; BSA, bovine serum albumin; CAS9, CRISPR-associated protein 9; CCPs, clathrin coated pits; CRISPR, clustered regularly interspaced short palindromic repeats; DAPI, 4′,6-diamidino-2-phenylindole; DMEM, Dulbecco modified Eagle medium; ECL, enhanced chemiluminescence; EGTA, ethylene glycol-bis(β-aminoethyl ether)-*N*,*N*,*N*′,*N*′-tetraacetic acid; FAC, ferric ammonium citrate; gRNA, guidanceRNA; HEPES, 2-[4-(2-hydroxyethyl)piperazin-1-yl]ethanesulfonic acid; HIF, hypoxia inducible factor; HMA, heterodimer migration analysis; IRE, iron regulatory elements; IRPs, iron regulatory proteins; JACoP, just another colocalization plugin; KD, knocked down; KO, knock out; LIP, labile iron pool; MARCH, membrane-associated RING-CH; MIUR, Ministry of University and Research; NTBI, non transferrin bound iron; PBS, phosphate buffered saline; PCR, polymerase chain reaction; PMSF, phenylmethylsulfonyl fluoride; SD, standard deviation; SDS–PAGE, sodium dodecyl sulfate polyacrylamide gel electrophoresis; siRNA, small interfering RNA; STR, short tandem repeat; TBS, tris buffered saline; Tf, transferrin; TfR1, transferrin receptor.

INTRODUCTION

Iron is required for key cellular functions but can participate in the generation of oxidants; therefore, cellular iron traffic must be carefully balanced (Gammella *et al*., 2016).

Transferrin receptor (TfR1) mediates the uptake of transferrin (Tf), the protein that binds circulating iron and delivers it to cells (Hamilton *et al*., 1979; Omary and Trowbridge, 1981; Brandsma *et al*., 2011). TfR1 is synthesized as a monomer but rapidly forms a homodimer that can bind one Tf molecule at each subunit (Ponka and Lok, 1999; Aisen, 2004). Importantly, the iron status of Tf influences its affinity for TfR1, as diferric (holo)Tf has an affinity for the TfR1 several fold higher than that of apo-Tf (Young *et al*., 1984). Upon binding at the cell surface, the complex of (holo)Tf and TfR1 is taken into cells through an extensively characterized process of clathrin-mediated endocytosis (Kirchhausen *et al*., 2014; Robinson, 2015), which begins with the formation of clathrin-coated pits (CCPs) on the cell surface (Mayle *et al*., 2012; Kirchhausen *et al*., 2014) and requires the adaptor protein AP2 (McMahon and Boucrot, 2011; Kirchhausen *et al*., 2014; Robinson, 2015); subsequently, TfR1 is internalized and trafficked to early endosomes. As a consequence of vesicle acidification, iron is released from Tf and transported to

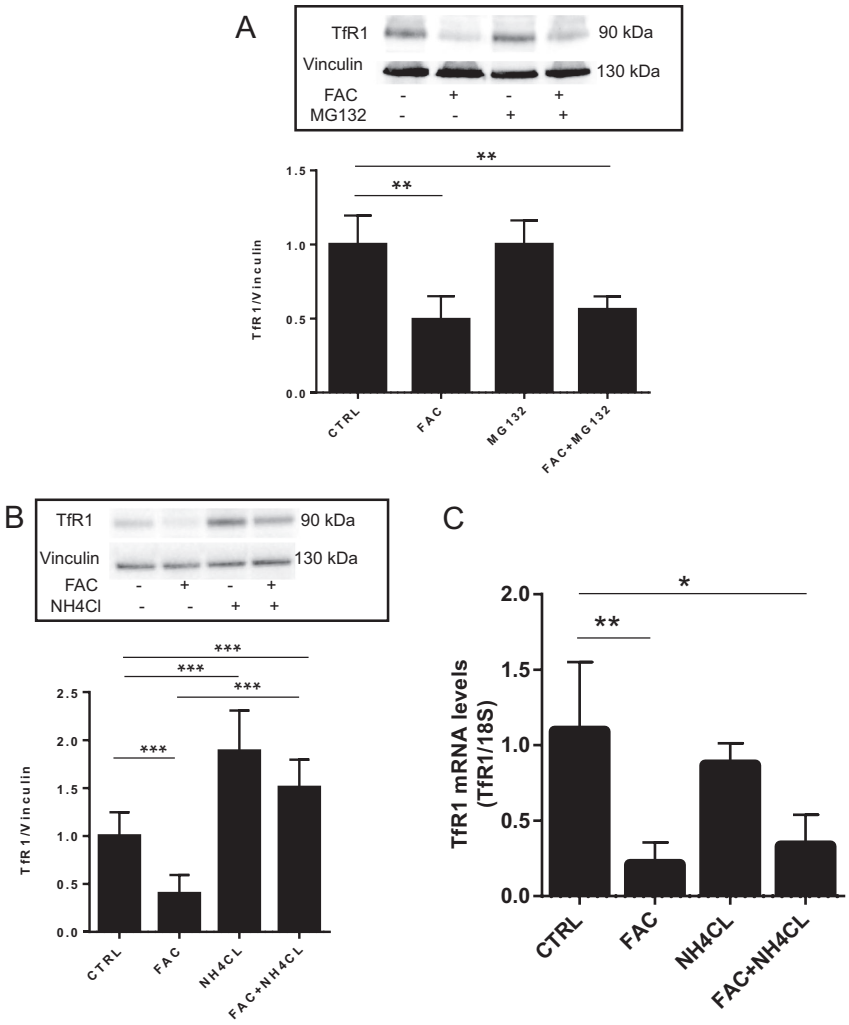

FIGURE 1: Lysosomal activity is required for iron-dependent down-regulation of TfR1. (A) Densitometric quantification and representative immunoblots of TfR1 levels in HepG2 cells left untreated or treated with FAC, MG132, or both. The values, normalized to vinculin, are expressed as a fraction of untreated cells. (B) Densitometric quantification and representative immunoblots of TfR1 levels in HepG2 cells left untreated or treated with FAC, NH_4Cl, or both. The values, normalized to vinculin, are expressed as a fraction of untreated cells. (C) TfR1 mRNA levels in cells treated as described for B. Samples in triplicate were normalized to the housekeeping gene 18S and expressed as a fraction of control cells. Data are presented as mean values ± SD. $^*P < 0.05$, $^{**}P < 0.01$, $^{***}P < 0.001$, $n = 5$ independent experiments.

the cytoplasm, while Tf and TfR1 are recycled back to the cell surface through recycling endosomes (Ullrich *et al.*, 1996) in a process requiring the action of sorting nexin 3 (Chen *et al.*, 2013). The last process of the TfR1 endocytic cycle involves the trafficking protein Sec15l1 (Lim *et al.*, 2005) that permits apo-Tf release to the bloodstream, while TfR1 is available to recapture iron-loaded Tf.

Because the number of TfR1 molecules is the rate-limiting step for iron entry into cells, TfR1 expression is finely regulated at multiple levels (Gammella *et al.*, 2017). TfR1 transcription is activated by hypoxia-inducible factors in iron-deprived cells (Bianchi *et al.*, 1999), and TfR1 mRNA levels are modulated by the iron regulatory proteins (IRP1 and IRP2), which control intracellular iron metabolism by regulating at the posttranscriptional level the expression of genes coding for proteins involved in iron uptake, utilization, storage, and export (Recalcati *et al.*, 2010). When the cellular labile iron pool (LIP) is scarce, active IRPs bind to iron-responsive elements (IREs) and stabilize TfR1 mRNA, thus increasing iron uptake and decreasing translation of mRNAs for ferritin, the iron storage protein. Conversely, in cells exposed to iron, the IRP activity is decreased, leading to reduced TfR1 mRNA stability and efficient ferritin mRNA translation, ultimately enhancing iron sequestration over uptake (Rouault, 2006; Gammella *et al.*, 2017).

Whether posttranslational mechanisms are involved in iron-mediated down-regulation of TfR1 levels is largely unknown, although it has been shown that the lysosomal degradation of TfR1 in glioma cells is accelerated by iron (Tachiyama *et al.*, 2011).

The aim of this study was to explore the possibility that changes in iron availability affect the TfR1 endocytic cycle and TfR1 protein stability in hepatic cells.

RESULTS AND DISCUSSION

Iron-dependent TfR1 down-regulation involves lysosomal degradation

TfR1 represents the major cellular entry for iron and its expression is finely regulated at multiple levels to keep cellular iron levels sufficient to maintain metabolic needs but below the threshold that facilitates oxidative stress (Gammella *et al.*, 2017). To study the mechanisms underlying iron-mediated TfR1 degradation, we treated HepG2 cells with 100 µg/ml ferric ammonium citrate (FAC) in the presence of specific inhibitors of different degradation pathways.

TfR1 protein levels were decreased by approximately 50% after 16 h of FAC treatment and thedown-regulation was observed also when cells were treated with the proteasomal inhibitor MG132, whereas exposure to MG132 alone had no significant effect (Figure 1A). These findings thereby indicate that the proteasome is not involved in the iron-dependent down-regulation of TfR1.

Conversely, incubation with NH_4Cl, a specific inhibitor of lysosomal activity, prevented the iron-dependent decrease in TfR1 in FAC-treated cells, restoring basal TfR1 levels (Figure 1B), thereby indicating that lysosomes are involved in FAC-mediated TfR1 degradation. Compared with control, TfR1 mRNA levels were down-regulated in FAC-treated cells, as expected according to the posttranscriptional control by the IRE/IRP pathway (Rouault, 2006; Recalcati *et al.*, 2010), but the presence of NH_4Cl did not rescue TfR1 mRNA expression (Figure 1C).

Because the TfR1 half-life is relatively long (6–14 h), probably only a small proportion of TfR1 is physiologically targeted for degradation in basal conditions; iron-induced TfR1 protein down-regulation by means of lysosomal degradation may represent a posttranslational control to reduce TfR1 surface levels via endocytosis, thus limiting iron uptake, a response that parallels the IRE-IRP–dependent posttranscriptional regulation.

Iron-mediated TfR1 degradation is independent of transferrin and H-ferritin

TfR1 is constitutively internalized, that is, independently of Tf binding (Ponka and Lok, 1999); however, regulation of TfR1

endocytosis by Tf was suggested by studies showing that the binding of Tf activates Src kinase, which phosphorylates components of the endocytic machinery like dynamin 2 and its actin-associated binding partner cortactin (Cao *et al.*, 2010), thus facilitating the internalization of the Tf-TfR1 complex. Moreover, the addition of FAC may increase the amount of (holo)Tf, which has a higher affinity for the TfR1 than apo-Tf (Young *et al.*, 1984).

We therefore decided to further investigate whether FAC is inducing TfR1 degradation through its binding to Tf. To this aim, 1) we performed experiments in HeLa cells, in which endogenous Tf was undetectable (Figure 2A), and we found results superimposable to those obtained in HepG2 cells, thus showing that FAC-mediated TfR1 lysosomal degradation was retained in this cell line not expressing Tf (Figure 2B); 2) we analyzed TfR1 degradation in HepG2 cells in which Tf has been knocked down (KD; 80–90% efficiency) (Figure 2C); FAC was able to induce TfR1 degradation in a lysosome-dependent manner also in the absence of Tf (Figure 2C). Experiments 1 and 2 were performed upon serum deprivation in order to avoid the presence of Tf in the culture medium. Overall, these data indicate that FAC-mediated TfR1 degradation in lysosomes does not require Tf. Notably, the Tf-independent pathway described here should mirror an in vivo condition characterized by the presence of non–Tf-bound iron (NTBI), as occurs in typical iron overload diseases (Brissot *et al.*, 2012), in which the buffering capacity of Tf is overwhelmed and iron enters the cells by means of Tf-independent pathways mediated by other transporters.

We then explored the possibility that the effect of iron is exerted through ferritin, a spherical molecule composed of 24 subunits of two types, H and L, that stores intracellular iron but is also secreted into circulation via a nonclassical lysosomal secretion pathway (Truman-Rosentsvit *et al.*, 2018). In fact, iron-bound H-ferritin was shown to bind TfR1 and direct its endocytosis toward a degradative fate in the lysosome (Li *et al.*, 2010). Thus, it could be hypothesized that the excess of iron increases H-ferritin synthesis and secretion, in turn stimulating TfR1 endocytosis and degradation. Indeed, as expected, FAC strongly induced H-ferritin (Figure 2D). To explore this hypothesis, we performed experiments in HepG2 cells in which H-ferritin has been knocked down (KD; 80–90% of efficiency) (Figure 2D). FAC treatment caused a decrease of TfR1 protein levels preventable by NH_4Cl also in these cells (Figure 2D), suggesting that iron-mediated TfR1 lysosomal degradation is largely independent of H-ferritin. H-ferritin knockdown triggered a strong decrease in basal TfR1 levels, possibly due to LIP expansion caused by the lack of iron storage inside ferritin, as reported in mice with H-ferritin gene deletion (Vanoaica *et al.*, 2010).

We assessed the role of H-ferritin also in HeLa cells in which H-ferritin has been stably knocked out using CRISPR-Cas9 methodology and that also showed a strong decrease in basal TfR1 levels. The lack of effect of H-ferritin ablation on FAC-induced TfR1 degradation was confirmed also in this model system (Supplemental Figure S1).

Iron-mediated TfR1 degradation and endocytosis proceeds also in AP2-depleted cells

Constitutive endocytosis of TfR1 occurs through CCPs and is mediated by the clathrin adaptor protein AP2, which plays an essential role in the process by recruiting clathrin to the plasma membrane and the cargo to the nascent CCP (Mettlen *et al.*, 2009; Cocucci *et al.*, 2012). Indeed, it has been shown that AP2 is essential for TfR1 constitutive internalization and recycling (Hinrichsen *et al.*, 2003; Motley *et al.*, 2003; Huang *et al.*, 2004; Mettlen *et al.*, 2009; Boucrot *et al.*, 2010; Liu *et al.*, 2010). To evaluate whether iron-induced TfR1 down-regulation depends on the canonical AP2-mediated endocytic pathway, we depleted the AP2μ subunit from HepG2 cells. Immunoblot analysis (Figure 3A) showed that TfR1 basal levels are increased in cells in which AP2μ was knocked down (AP2 KD; 80–90% efficiency), possibly because of accumulation of the protein at the plasma membrane (see below) and ensuing stabilization. Exposure to FAC reduced TfR1 protein levels also in AP2 KD cells, though not restoring the TfR1 levels observed in control cells, thus showing that AP2 is not absolutely required for ion-induced TfR1 degradation. As the control, we evaluated TfR1 mRNA levels (Figure 3B) and we observed a decrease in both control and AP2 KD cells, which was not rescued by NH_4Cl treatment, in line with the results shown in Figure 1C.

To investigate whether FAC treatment induced TfR1 degradation by increasing its endocytosis, we measured the number of TfR1 molecules at the plasma membrane through an ^{125}I-Tf–based saturation binding assay in the different conditions. FAC treatment caused a significant decrease in the number of TfR1 molecules in control cells (Figure 3C), suggesting that FAC is inducing TfR1 internalization and degradation. In AP2 KD cells the number of TfR1 molecules at the cell membrane was 10fold higher than in control cells, in line with the results of Figure 3A and with the block of constitutive clathrin-mediated endocytosis of TfR1 in this condition. Notably, FAC treatment was able to reduce the number of TfR1 molecules at the cell surface also in AP2 KD cells, albeit not to the level observed in control cells (Figure 3C).

We complemented these experiments by performing ^{125}I-Tf–based internalization assays at the initial rate and measuring the endocytic rate constant in the various conditions. The experiments showed that FAC treatment in control cells increased the Tf endocytic rate, whereas AP2 KD almost completely blocked Tf internalization, confirming previous observations (Hinrichsen *et al.*, 2003; Motley *et al.*, 2003; Huang *et al.*, 2004; Mettlen *et al.*, 2009; Boucrot *et al.*, 2010; Liu *et al.*, 2010). This endocytic block was partially rescued by FAC treatment (Figure 3D). The increase in the Tf internalization rate is quantitatively similar in control and in AP2 KD cells (2–2.5-fold), suggesting that FAC is able to induce TfR1 endocytosis through a pathway that is largely AP2-independent. These data also showed that, although Tf is not required for FAC-mediated TfR1 endocytosis, in a condition that mimics iron overload, the Tf-TfR1 complex is targeted by FAC for internalization also through an AP2-independent pathway that directs the receptor to lysosomal degradation, thus suggesting that iron availability is a critical regulator of TfR1 endocytosis and trafficking.

The iron-dependent trafficking of TfR1 to the lysosome follows an AP2- and transferrin-independent pathway

To visualize endocytosis and trafficking of TfR1 in the various conditions, we labeled TfR1 at 4°C with an antibody directed against the extracellular domain, and internalization of the antibody/TfR1 complex was allowed at 37°C in cells treated or not with FAC. At time zero ($T = 0$), the TfR1 signal was localized at the cell membrane and was stronger in AP2 KD cells than in control cells, confirming that TfR1 in the absence of FAC is internalized via the canonical constitutive endocytic pathway and is accumulated at the plasma membrane upon AP2 depletion (Figure 4A). In untreated cells, after 16 h at 37°C TfR1 was subjected to multiple cycles of endocytosis and recycling and accumulated in intracellular compartments with only limited colocalization with the lysosomal marker Lamp-1, in agreement with the fact that in basal conditions TfR1 is mostly recycled and not targeted to degradation (Mayle *et al.*, 2012). Conversely, in cells treated with FAC the TfR1 signal was present in big intracellular

dots extensively colocalizing with Lamp-1, as shown by colocalization quantification (Figure 4C), confirming that in this condition TfR1 is trafficking toward the lysosomes. Importantly, FAC treatment increased the lysosomal localization of TfR1 also in AP2 KD cells, confirming that AP2 is not necessary for iron-induced lysosomal targeting and degradation of TfR1. The accumulation of TfR1 in Lamp-1–positive compartments in both control and AP2 KD cells was also observed upon treatment for 16 h with NH_4Cl in the presence of FAC (Figure 4, A and C)), confirming that FAC induces an AP2-independent endocytic mechanism that targets TfR1 to the lysosomes.

These results were confirmed by experiments in which we used bafilomycin A1, another lysosomal inhibitor. The experiments reported in Figure 4, B and C, showed that exposure to bafilomycin A1 in the presence of FAC led to accumulation of TfR1 in lysosomes. Western blot analysis showed that incubation with bafilomycin A1 prevented the iron-dependent decrease in TfR1 in FAC-treated cells, restoring basal TfR1 levels (Figure 4D), in line with the results obtained using NH_4Cl (Figure 1).

To better evaluate the effect of iron on endocytic uptake, we analyzed the internalization of the antibody/TfR1 complex at shorter incubation times (Figure 5A). Even after 3 h, FAC treatment induced the internalization of TfR1, but colocalization with Lamp-1 was not evident (Figure 5B), suggesting that 3 h is not sufficient for a significant accumulation of TfR1 in lysosomes.

We also confirmed that the lysosomal TfR1 degradation induced by FAC is Tf-independent by showing that the lysosomal TfR1 localization in Tf KD cells was similar to that occurring in control cells, both in basal conditions and after FAC treatment. Moreover, no differences were observed between AP2 KD cells and cells with double KD for Tf and AP2 (Supplemental Figure S2).

Given the extensive characterization of its cycling pathway and its independence on ligand binding, TfR1 has been widely used to study the mechanisms of constitutive endocytosis, often not considering its physiological function in iron metabolism. Here, we showed that an excess of iron in the form of FAC induces TfR1 internalization mainly through a pathway that is independent of Tf, H-ferritin, and AP2 and targets the receptors to lysosomal degradation, thus suggesting that iron availability is a critical regulator of TfR1 endocytosis and trafficking. Our model should mirror the in vivo condition characterized by the presence of NTBI that occurs in iron overload diseases. However, how NTBI regulates TfR1 endocytosis remains an open question. Iron could—directly or indirectly—regulate factors involved in TfR1 endocytosis and degradative pathway, for example, via direct interaction or through transcriptional up-regulation. For example, MARCH8, a member of the MARCH family of E3 (cited in Funakoshi *et al.*, 2014), has been previously shown to be involved in TfR1 lysosomal degradation (Fujita *et al.*, 2013). However, we found that TfR1 was still down-regulated upon FAC treatment in cells silenced for MARCH8 (Supplemental Figure S3). Therefore, in our cell model system, the lysosomal degradation of TfR1 is MARCH8-independent.

Cellular iron overload can promote oxidative stress and ferroptosis, a regulated form of cell death that is to some extent controlled by autophagy and depends on correct lysosomal function, which is important for cellular iron homeostasis and iron uptake (Nakamura *et al.*, 2019). We cannot currently exclude that these mechanisms could be involved in the lysosomal targeting of TfR1.

On the other hand, we cannot currently rule out that the higher amount of iron could trigger a transcriptional response mediated by hypoxia-inducible factors (HIF). Indeed, it has been shown that HIF2α is inhibited by ferrous iron (Schwartz *et al.*, 2019) and exposure to FAC may end up in an increased content of ferrous iron thanks to reductases that may assist iron transporters like DMT1 or members of the ZIP family. However, it has been suggested that endocytosis is facilitated by hypoxia and hence elevated HIF activity (reviewed in López-Hernández *et al.*, 2020). This mechanism, therefore, does not seem to apply to the situation described in the present study.

Alternatively, the excess of iron, in addition to regulating the initial internalization step (see Figure 3C), may also act at the postinternalization level, at the sorting step. Indeed, it has been shown that Rab12 is involved in the constitutive routing of TfR1 from recycling endosomes to lysosomes for degradation (Matsui *et al.*, 2011). Thus, one possibility is that iron overload enhances the constitutive degradative pathway of TfR1, which normally represents only a minor route, thus preventing excessive intracellular iron accumulation. This possibility requires future investigations. In addition, the nature of the AP2-independent endocytic mechanism also needs a deeper analysis in order to clarify whether it belongs to the previously described clathrin-independent mechanisms (Johannes *et al.*, 2015; Caldieri *et al.*, 2018; Thottacherry *et al.*, 2019; Casamento and Boucrot, 2020).

In conclusion, we have characterized a novel regulatory mechanism of TfR1 expression based on an unconventional endocytic pathway that redirects TfR1 toward the lysosome. This mechanism acts in conditions of iron overload to promptly down-regulate cell surface TfR1 levels, in parallel to the well-characterized post-transcriptional regulation of TfR1 mRNA stability (Rouault, 2006; Gammella *et al.*, 2017), thus avoiding detrimental effects caused by the excess of intracellular iron. In particular, given its independency of Tf, this novel mechanism could be critical to limit uncontrolled iron ingress into liver cells under conditions of systemic iron overload when NTBI is present. Recently, an increased return of endocytosed TfR1 back to the plasma membrane under conditions of iron deprivation has been reported, a mechanism likely representing an attempt to retrieve more iron (Jonker *et al.*, 2020). Likewise, the present findings provide further evidence for the conclusion that modulating TfR1 cycling should be considered one of the numerous mechanisms maintaining appropriate cellular iron levels.

MATERIALS AND METHODS

Request a protocol through Bio-protocol.

Cell culture

HepG2 human hepatoma cells and HeLa cells (American Type Culture Collection) were routinely maintained in DMEM containing 10% fetal calf serum and 1% glutamine at 37°C in 5% CO_2. The H-ferritin-knockout HeLa cell line (HeLa KO) was generated by CRISPR/Cas9 technology as previously described (Truman-Rosentsvit *et al.*, 2018). Briefly, the sequence of the guidanceRNA (gRNA) designed to uniquely target the FTH gene within the genome was FTH (exon 1)—GACCATGGACAGGTAAACGT. HeLa cells were transfected with an all-in-one expression plasmid for simultaneous gRNA and Cas9 expression (Addgene plasmid #42230), and clonal colonies were screened for H-ferritin expression by Western blot. Genomic alterations were checked by heterodimer migration analysis (HMA) and then confirmed by Sanger DNA sequencing. As negative control, we used mock-treated cells.

For the various treatments, cells maintained in serum-free conditions were incubated for 16 h in the presence or absence of 100 μg/ml ferric ammonium citrate (FAC); 1 μM MG132, 20 mM NH_4Cl, or 10 nM bafilomycin A1 (Sigma, Milan, Italy) was added for

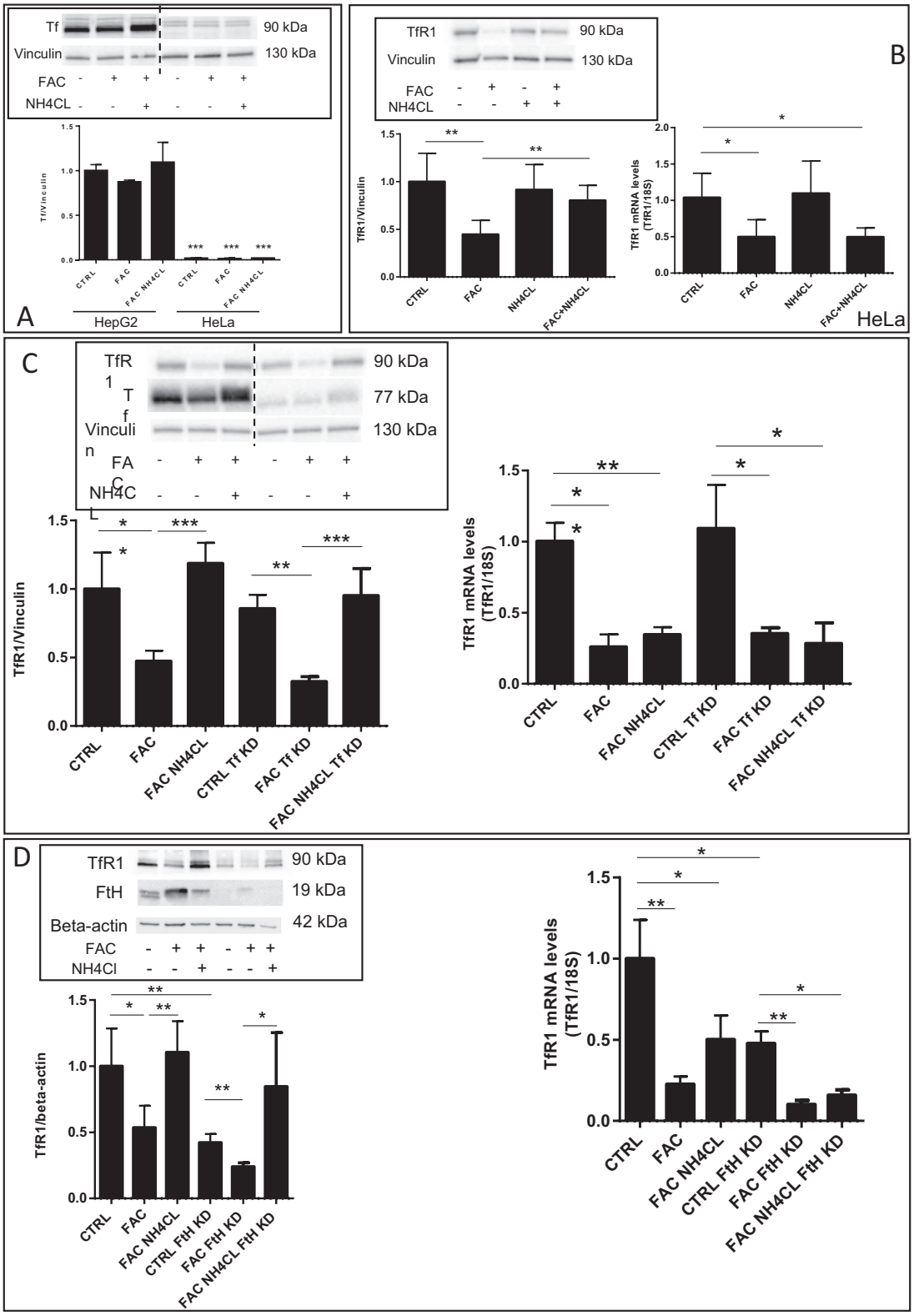

FIGURE 2: Iron-dependent TfR1 degradation is independent of Tf and H-ferritin. (A) Densitometric quantification and representative immunoblots of Tf levels in HepG2 and HeLa cells untreated or treated with FAC or a combination of FAC and NH_4Cl. The immunoblot panel was assembled from samples run on the same gel by splicing out the irrelevant lanes (as shown by the dotted line). The values, normalized to vinculin, are expressed as a fraction of untreated cells. (B) Left, Densitometric quantification and representative immunoblots of TfR1 levels in HeLa cells treated as described for Figure 1B. The values, normalized to vinculin, are expressed as a fraction of untreated cells. Right, TfR1 mRNA levels in HeLa cells treated as described in Figure 1B. Samples in triplicate were normalized to the housekeeping gene 18S and expressed as a fraction of control cells. (C) Left, Densitometric quantification and representative immunoblots of TfR1 and Tf levels in HepG2 cells mock-transfected or transfected with siRNA targeting Tf (Tf KD) and treated as

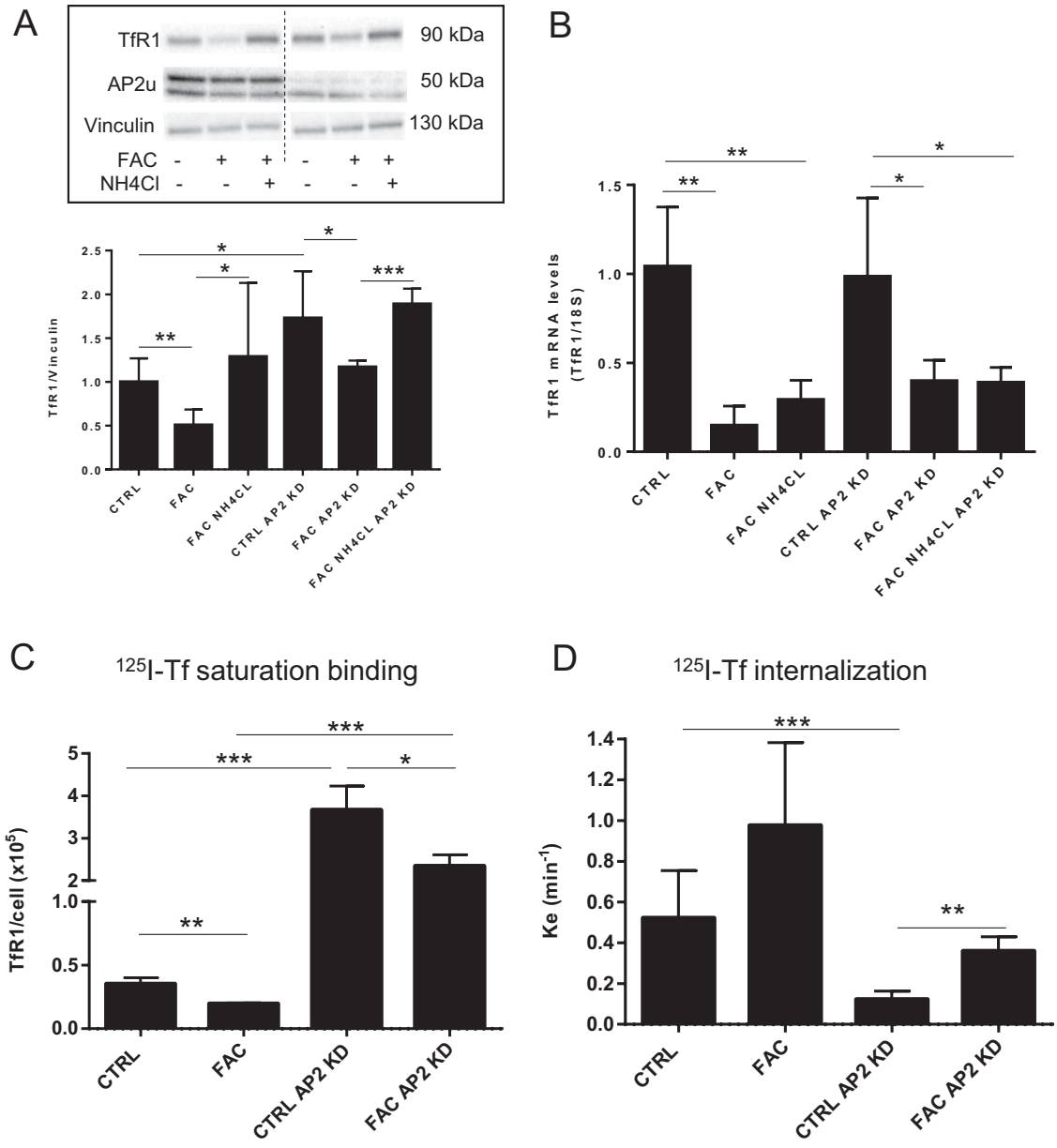

FIGURE 3: Iron-dependent TfR1 degradation is independent of AP2. (A) Densitometric quantification and representative immunoblots of TfR1 and AP2μ levels in HepG2 cells mock-transfected or transfected with a siRNA targeting AP2μ (AP2 KD) and treated as described in Figure 2A. The immunoblot panel was assembled from samples run on the same gel by splicing out the irrelevant lanes (as shown by the dotted line). The value of TfR1, normalized to vinculin, is expressed as a fraction of control. (B) TfR1 mRNA levels in HepG2 cells transfected and treated as described in Figure 2A. Samples in triplicate were normalized to the housekeeping gene 18S and expressed as a fraction of control cells. (C) ^{125}I-Tf saturation binding in HepG2 cells mock-transfected or transfected with siRNA targeting AP2μ (AP2 KD) and either left untreated or treated with FAC. The surface TfR1 number/cell is reported. (D) ^{125}I-Tf internalization rate was followed at early times (2, 4, 6 min) in HepG2 cells treated with FAC for 16 h as in C. Internalization constants (Ke) are reported. Data are presented as mean values ± SD. *$P < 0.05$, ** $P < 0.01$, *** $P < 0.001$, $n = 3$ for B, C, and D; $n = 5$ for A.

described in A. The immunoblot panel was assembled from samples run on the same gel by splicing out the irrelevant lanes (as shown by the dotted line). The values of TfR1 and Tf, normalized to vinculin, are expressed as a fraction of control. Right, TfR1 mRNA levels in HepG2 cells transfected and treated as described above. Samples in triplicate were normalized to the housekeeping gene 18S and expressed as a fraction of control cells. (D) Left, Densitometric quantification and representative immunoblots of TfR1 and Ft-H levels in HepG2 cells mock-transfected or transfected with siRNA targeting Ft-H (Ft-H KD) and treated as described in A. The values of TfR1 and Ft-H, normalized to β-actin, are expressed as a fraction of control. Right, TfR1 mRNA levels in HepG2 cells transfected and treated as described above. Samples in triplicate were normalized to the housekeeping gene 18S and expressed as a fraction of control cells. Data are presented as mean values ± SD. * $P < 0.05$, **$P < 0.01$, *** $P < 0.001$, $n = 3$.

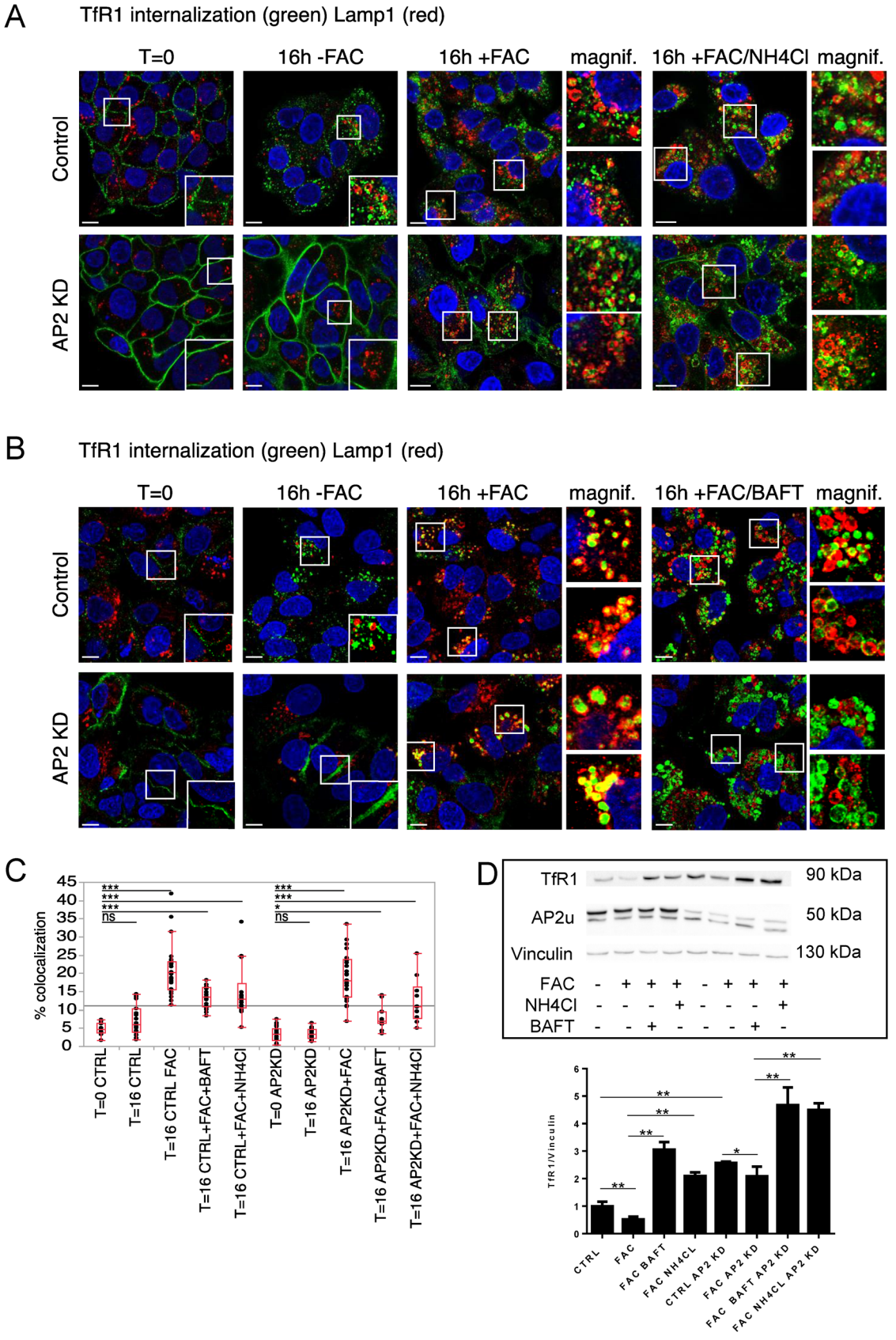

FIGURE 4: Iron-mediated lysosomal targeting of TfR1 follows an AP2-independent endocytic pathway. (A, B) Confocal images of HepG2 cells mock-transfected or transfected with siRNA targeting AP2μ (AP2 KD). The cells were labeled with anti-TfR1 at 4°C ($T = 0$) and then left at 37°C for 16 h untreated or treated with FAC, a combination of FAC and

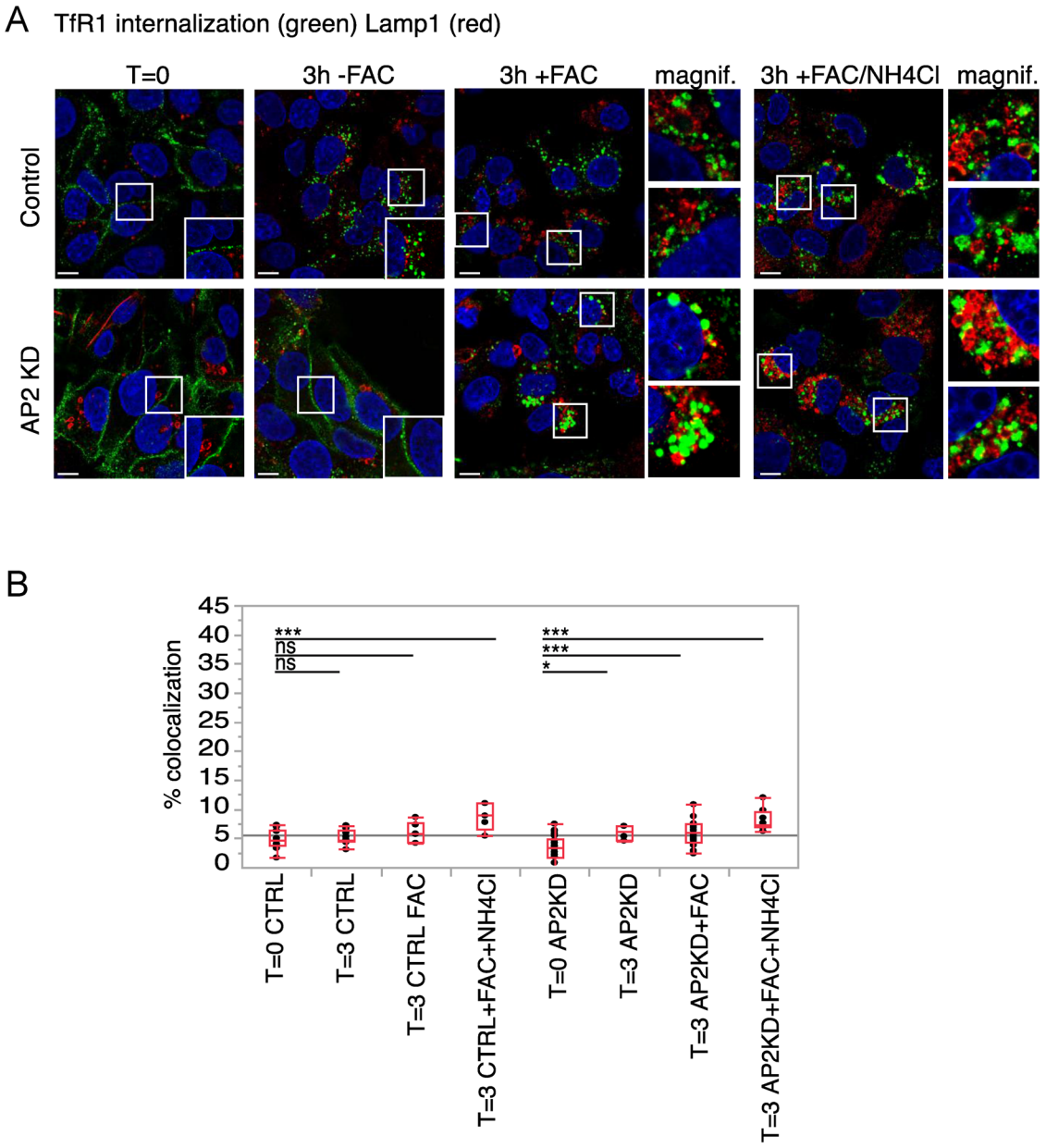

FIGURE 5: Iron-mediated TfR1 endocytic uptake at short incubation time. (A) Confocal images of HepG2 cells mock-transfected or transfected with siRNA targeting AP2μ (AP2 KD). The cells were treated for 16 h with or without FAC, labeled with anti-TfR1 at 4°C ($T = 0$) for 1 h, and left at 37°C for 3 h untreated or treated with FAC or with a combination of FAC and NH_4Cl. Cells were then fixed and processed for immunofluorescence staining. TfR1 (green) and Lamp-1 (red) are shown. Nuclei were DAPI-stained. The indicated cropped areas are shown in the insets or at the right. Bars, 10 μm. (B) Quantification of percentage of colocalization of TfR1 (green) and Lamp-1 (red). $n = 2$; at least four fields of view per sample were used for quantification of percentage of colocalization between TfR1 and Lamp1. $^*P < 0.05$; $^{***}P < 0.001$; ns: not significant.

NH_4Cl (A), or a combination of FAC and bafilomycin A1 (BAFT, 10 nM, B). Cells were then fixed and processed for immunofluorescence staining. TfR1 (green) and Lamp-1 (red) are shown. Nuclei were DAPI-stained. The indicated cropped areas are shown in the insets or at the right. Bars, 10 μm (C) Quantification of percentage of colocalization of TfR1 (green) and Lamp-1 (red). $n = 3$; at least 10 fields of view per sample were used for quantification of percentage of colocalization between TfR1 and Lamp1. $^*P < 0.05$; $^{***}P < 0.001$; ns: not significant. (D) Densitometric quantification and representative immunoblots of TfR1 and AP2μ levels in HepG2 cells mock-transfected or transfected with siRNA targeting AP2μ (AP2 KD) and left untreated or treated with FAC, a combination of FAC and NH_4Cl, or a combination of FAC and bafilomycin (BAFT). The values of TfR1 and AP2μ, normalized to vinculin, are expressed as a fraction of control. Data are presented as mean values ± SD. $^*P < 0.05$, $^{**}P < 0.01$, $n = 3$.

3 or 16 h. Cells were authenticated by STR profiling (StemElite ID System; Promega, Milan, Italy) and tested for mycoplasma at each batch freezing by PCR56 and biochemical assay (MycoAlert; Lonza Euroclone, Pero, Italy).

RNA interference

RNA interference (RNAi) was performed using the LipofectAMINE RNAi MAX reagent from Invitrogen (Monza, Italy), according to the manufacturer's instructions. For AP2 knockdown, cells were subjected to a single reverse transfection, treated with 8 nM small interfering RNA (siRNA) oligo, and analyzed 5 d after transfection. For Tf, H-ferritin, and MARCH8 knockdown, cells were subjected to a double reverse transfection, treated with 8 nM siRNA oligos, and analyzed 5 d after transfection. As a negative control, we used mock-treated cells transfected with a pool of negative control oligos (Riboxx; Euroclone, Pero, Italy).

Oligo sequences:

AP2μ (Riboxx): 5′-UGACCCGAAAGGCAUCCACCCCC-3′;

Tf, pool of three oligos (Riboxx): 5′-UUAAUGAUCACG-CAGACCCCC-3′

5′-UCAUUCAGAUUCUUAGCCCCC-3′

5′-UAUUCAUCUACCGGCUUCCCCC-3′;

H-ferritin pool of three oligos (Riboxx): 5′-UUUCUCAGCAU-GUUCCCUCCCCC-3′

5′-UUCAUUAUCACUGUCUCCCCC-3′

5′-UAGAACUGAACAACGGCACCCCC-3′

MARCH8 pool of three oligos (Riboxx): 5′-UAUAAAUAGUCAC-CUGUCCCCC-3′

5′-AUUCUGUUCUUCCCUCUCCCCC-3′

5′-AUGAGCACAUACAAGGACCCCC-3′

Quantitative real-time PCR

Total RNA isolated from HepG2 and HeLa cells using the TRI reagent (Sigma, Milan, Italy) was reverse transcribed into cDNA with the Proto Script M-MuLV First Strand cDNA Synthesis Kit (New England Biolabs, Euroclone; Pero, Italy), and the obtained cDNA served as a template for real-time PCR, based on the TaqMan methodology (Life Technologies, Monza, Italy). Thermal cycling parameters were 40 cycles at 95°C for 15 s and 60°C for 1 min. Each sample was amplified in triplicate using the primers for TfR1 and 18s rRNA and the amount of TfR1 RNA was calculated using the 2^{-DCt} method and normalized to 18S rRNA.

Immunofluorescence

Cells seeded on glass coverslips and maintained in the presence or absence of 100 μg/ml FAC alone or in combination with 20 mM NH_4Cl or 10 nM bafilomycin A1 were incubated with the anti-TfR1 antibody (DF1513; Thermo Scientific; 1:50 dilution) for 1 h on ice in order to inhibit endocytosis. The medium containing the antibody was then eliminated, and prewarmed medium with or without FAC, and/or NH_4Cl, and/or bafilomycin A1 was added. One sample (time 0) was immediately fixed in paraformaldehyde (see below) after the incubation on ice with the antibody. The other samples were then incubated at 37°C for 16 h. At the end of treatment, cells were fixed in 4% paraformaldehyde (in 1× phosphate-buffered saline [PBS]) for 10 min at room temperature and washed with 1× PBS.

To analyze TfR1 endocytic uptake at short incubation times, the cells were treated or not with 100 μg/ml FAC for 16 h. The next day, cells were incubated with anti-TfR1 antibody (DF1513; Thermo Scientific; 1:50 dilution) for 1 h on ice. The medium containing the antibody was then eliminated and prewarmed medium with or without FAC and/or NH_4Cl was added for 3 h.

Permeabilization was performed with 1× PBS in the presence of 2% bovine serum albumin (BSA) and 0.1% saponin for 30 min at room temperature. Next, cells were incubated at room temperature for 1 h with the antibody against Lamp1 (rabbit polyclonal from Santa Cruz' DBA Italia, Segrate, Milan, Italy; 1:100 in 1× PBS, 0.2% BSA, 0.1% saponin), washed three times with 1× PBS containing 0.1% saponin, and incubated for 40 min with fluorescently labeled secondary antibodies anti-rabbit 1:200 (647-Alexa,; Invitrogen; to label Lampl) and anti-mouse 1:200 (488-Alexa; Invitrogen; to label TfR1). Nuclei were 4′,6-diamidino-2-phenylindole (DAPI)-stained for 5 min in 1× PBS, BSA 0.2%, saponin 0.1%. After three washes with PBS, coverslips were subjected to postfixation in 4% paraformaldehyde (in 1× PBS) for 10 min, washed again in PBS, and immediately mounted with glycerol. Images were obtained using a Leica TCS SP2 or TCS SP2 AOBS confocal microscope equipped with a 63× oil objective and processed using ImageJ and Adobe Photoshop software (Adobe).

The percentage of colocalization between TfR1 and Lamp1 was quantified through JACoP (Just Another Colocalization Plugin) Plugin software on ImageJ. Statistical analysis was performed on JMP software, Each Pair Student's *t*-test two-tailed. Quantitative data are presented as box plots. Each box plot is defined by 25 and 75 percentiles showing median, whiskers representing 10 and 90 percentiles, and outliers if present.

Immunoblot analysis

Cells were directly lysed on a plate in a buffer containing 50 mM HEPES, pH 7.5, 50 mM NaCl, 1.5 mM $MgCl_2$, 5 mM ethylene glycol-bis(β-aminoethyl ether)-*N*,*N*,*N*′,*N*′-tetraacetic acid (EGTA), 1% Triton X-100, 1% glycerol, plus protease inhibitor cocktail (Calbiochem; Sigma, Milan, Italy) and phosphatase inhibitors (20 mM sodium pyrophosphate, pH 7.5, 50 mM NaF, 2 mM phenylmethylsulfonyl fluoride (PMSF), 10 mM Na_3VO_4, pH 7.5), followed by clarification for 1 h at 120,000 × *g* for 45 min. Aliquots of supernatants containing the desired amount of proteins were loaded onto 1–1.5 mm-thick 8% SDS–PAGE gels for electrophoresis (Biorad; Segrate, Milan, Italy). Proteins were transferred to nitrocellulose (Schleicher and Schuell; Sigma, Milan, Italy). After the efficiency of protein transfer was determined by Ponceau staining, the filters were blocked for 1 h in 5% milk in TBS supplemented with 0.1% Tween (TBS-T). After blocking, filters were incubated with primary antibodies against TfR1 (Invitrogen, Monza, Italy; 1:500 dilution), Tf (Invitrogen, Monza, Italy; 1:1000), H-ferritin (Cell Signalling; Euroclone, Pero, Italy; 1:1000), AP2μ (Transduction BD, Bioscience, DBA Italia, Segrate; 1:100 dilution), or vinculin (Sigma, Milan, Italy; 1:5000 dilution) and β-actin (Sigma, Milan, Italy; 1:500 dilution) diluted in TBS-T, 5% milk, for 1 h at room temperature, followed by three washes of 5 min each in TBS-T. Filters were then incubated with the appropriate horseradish peroxidase–conjugated secondary antibody (Cell Signalling; Euroclone, Pero, Italy; or BioRad; Segrate, Milan, Italy) diluted in TBS-T for 30 min. After the incubation with the secondary antibody, the filter was washed three times in TBS-T (5 min each) and the bound secondary antibody was revealed using the enhanced chemiluminescence (ECL) method (Amersham; Euroclone, Pero, Italy) and quantified using ImageLab 5.2.1 software, with the values being calculated after normalization to the amount of vinculin or β-actin.

Internalization assay

Internalization experiments were performed at 37°C without temperature shift as previously described (Caldieri *et al*., 2017). Briefly,

mock-treated cells and AP2μ KD cells were plated into 24-well plates (60,000 cells/well). Cells were plated in triplicate for each time point, plus one well for the unspecific binding. The next day, cells were serum-starved for at least 6 h in binding buffer (serum-free medium supplemented with 0.1% BSA, 20 mM HEPES) and then treated or not with 100 μg/ml FAC in binding buffer for 16 h. Cells were then incubated at 37°C in the presence of 2 μg of ^{125}I-Tf (PerkinElmer, Milan, Italy) in 300 μl of binding buffer. At different time points (2, 4, and 6 min), cells were put on ice, washed twice in cold PBS, and then incubated for 5 min at 4°C in 300 μl of acid wash solution (0.2 M acetic acid, 0.5 M NaCl, pH 2.5). Then, the solution was removed from the cells and the radioactivity was measured using a γ-counter. This sample represents the amount of ^{125}I-Tf bound to the receptor on the cell surface. Cells were left to dry at room temperature for 5 min and then lysed with 300 μl of 1 N NaOH. The lysate was collected, and the radioactivity was measured. This sample represents the amount of internalized ^{125}I-Tf. The unspecific binding was measured at each time point in the presence of a 500-fold excess of nonradioactive Tf. After being corrected for nonspecific binding, the rate of internalization was expressed as the ratio between internalized and surface-bound radioactivity.

Saturation binding assay

Saturation binding assays were performed as previously described (Sigismund *et al*., 2013). Briefly, mock-treated cells and AP2μ KD cells were plated into 24-well plates (60,000 cells/well). Cells were plated in triplicate for each time point, plus one well for the unspecific binding. The next day, cells were serum-starved for at least 6 h in binding buffer (serum-free medium supplemented with 0.1% BSA, 20 mM HEPES) and then treated or not with 100 μg/ml FAC in binding buffer. Cells were then incubated on ice for 6 h in the presence of 2 μg of ^{125}I-Tf (PerkinElmer, Milan, Italy) in binding buffer. Cells were then washed three times with ice-cold PBS and solubilized in 1 N NaOH. The number of TfR1 molecules/cell was deduced from the total recovered counts, corrected for the specific activity of the radioligand, and divided for the number of cells in the plate. Nonspecific binding was measured in the presence of a 500-fold excess nonradioactive Tf and subtracted from the total counts.

Statistical analysis

Results are expressed as mean ± SD, as specified. Statistical significance between groups was assessed by unpaired Student's *t* test with Prism software (version 6.00 for Windows; GraphPad).

ACKNOWLEDGMENTS

This work was supported by grants from the Italian Ministry of University and Scientific Research (MIUR) to S. S. (Prot. 2017E5L5P3) and Worldwide Cancer Research (16-1245) to S. S. A. C. was supported by a fellowship from the Fondazione Umberto Veronesi. I.S.L. was supported by an Associazione Italiana Ricerca sul Cancro (AIRC) fellowship. We thank Pier Paolo Di Fiore for helpful suggestions.

REFERENCES

Aisen P (2004). Transferrin receptor 1. Int J Biochem Cell Biol 36, 2137–2143.

Bianchi L, Tacchini L, Cairo G (1999). HIF-1-mediated activation of transferrin receptor gene transcription by iron chelation. Nucleic Acids Res 27, 4223–4227.

Boucrot E, Saffarian S, Zhang R, Kirchhausen T (2010). Roles of AP-2 in clathrin-mediated endocytosis. PLoS One 5, e10597.

Brandsma ME, Jevnikar AM, Ma S (2011). Recombinant human transferrin: beyond iron binding and transport. Biotechnol Adv 29, 230–238.

Brissot P, Ropert M, Le Lan C, Loréal O (2012). Non-transferrin bound iron: a key role in iron overload and iron toxicity. Biochim Biophys Acta 1820, 403–410.

Caldieri G, Barbieri E, Nappo G, Raimondi A, Bonora M, Conte A, Verhoef LGGC, Confalonieri S, Malabarba MG, Bianchi F, *et al* (2017). Reticulon 3-dependent ER-PM contact sites control EGFR nonclathrin endocytosis. Science 356, 617–624.

Caldieri G, Malabarba MG, Di Fiore PP, Sigismund S (2018). EGFR trafficking in physiology and cancer. Prog Mol Subcell Biol 57, 235–272.

Cao H, Chen J, Krueger EW, McNiven MA (2010). SRC-mediated phosphorylation of dynamin and cortactin regulates the "constitutive" endocytosis of transferrin. Mol Cell Biol 30, 781–792.

Casamento A, Boucrot E (2020). Molecular mechanism of fast endophilin-mediated endocytosis. Biochem J 477, 2327–2345.

Chen C, Garcia-Santos D, Ishikawa Y, Seguin A, Li L, Fegan KH, Hildick-Smith GJ, Shah DI, Cooney JD, Chen W, *et al.* (2013). Snx3 regulates recycling of the transferrin receptor and iron assimilation. Cell Metab 17, 343–352.

Cocucci E, Aguet F, Boulant S, Kirchhausen T (2012). The first five seconds in the life of a clathrin-coated pit. Cell 150, 495–507.

Fujita H, Iwabu Y, Tokunaga K, Tanaka Y (2013). Membrane-associated RING-CH (MARCH) 8 mediates the ubiquitination and lysosomal degradation of the transferrin receptor. J Cell Sci 126, 2798–2809.

Funakoshi Y, Chou MM, Kanaho Y, Donaldson JG (2014). TRE17/USP6 regulates ubiquitylation and trafficking of cargo proteins that enter cells by clathrin-independent endocytosis. J Cell Sci 127, 4750–4761.

Gammella E, Buratti P, Cairo G, Recalcati S (2017). The transferrin receptor: the cellular iron gate. Metallomics 9, 1367–1375.

Gammella E, Recalcati S, Cairo G (2016). Dual role of ROS as signal and stress agents: iron tips the balance in favor of toxic effects. Oxid Med Cell Longev 2016, 1–9.

Hamilton TA, Wada HG, Sussman HH (1979). Identification of transferrin receptors on the surface of human cultured cells. Proc Natl Acad Sci USA 76, 6406–6410.

Hinrichsen L, Harborth J, Andrees L, Weber K, Ungewickell EJ (2003). Effect of clathrin heavy chain- and alpha-adaptin-specific small inhibitory RNAs on endocytic accessory proteins and receptor trafficking in HeLa cells. J Biol Chem 278, 45160–45170.

Huang F, Khvorova A, Marshall W, Sorkin A (2004). Analysis of clathrin-mediated endocytosis of epidermal growth factor receptor by RNA interference. J Biol Chem 279, 16657–16661.

Johannes L, Parton RG, Bassereau P, Mayor S (2015). Building endocytic pits without clathrin. Nat Rev Mol Cell Biol 16, 311–321.

Jonker CTH, Deo C, Zager PJ, Tkachuk AN, Weinstein AM, Rodriguez-Boulan E, Lavis LD, Schreiner R (2020). Accurate measurement of fast endocytic recycling kinetics in real time. J Cell Sci 133, jcs231225.

Kirchhausen T, Owen D, Harrison SC (2014). Molecular structure, function, and dynamics of clathrin-mediated membrane traffic. Cold Spring Harb Perspect Biol 6, a016725.

Li L, Fang CJ, Ryan JC, Niemi EC, Lebrón JA, Björkman PJ, Arase H, Torti FM, Torti SV, Nakamura MC, *et al.* (2010). Binding and uptake of H-ferritin are mediated by human transferrin receptor-1. Proc Natl Acad Sci USA 107, 3505–3510.

Lim JE, Jin O, Bennett C, Morgan K, Wang F, Trenor CC, Fleming MD, Andrews NC (2005). A mutation in Sec15l1 causes anemia in hemoglobin deficit (hbd) mice. Nat Genet 37, 1270–1273.

Liu AP, Aguet F, Danuser G, Schmid SL (2010). Local clustering of transferrin receptors promotes clathrin-coated pit initiation. J Cell Biol 191, 1381–1393.

López-Hernández T, Haucke V, Maritzen T (2020). Endocytosis in the adaptation to cellular stress. Cell Stress 4, 230–247.

Matsui T, Itoh T, Fukuda M (2011). Small GTPase Rab12 regulates constitutive degradation of transferrin receptor. Traffic 12, 1432–1443.

Mayle KM, Le AM, Kamei DT (2012). The intracellular trafficking pathway of transferrin. Biochim Biophys Acta 1820, 264–281.

McMahon HT, Boucrot E (2011). Molecular mechanism and physiological functions of clathrin-mediated endocytosis. Nat Rev Mol Cell Biol 12, 517–533.

Mettlen M, Stoeber M, Loerke D, Antonescu CN, Danuser G, Schmid SL (2009). Endocytic accessory proteins are functionally distinguished by their differential effects on the maturation of clathrin-coated pits. Mol Biol Cell 20, 3251–3260.

Motley A, Bright NA, Seaman MN, Robinson MS (2003). Clathrin-mediated endocytosis in AP-2-depleted cells. J Cell Biol 162, 909–918.

Nakamura T, Naguro I, Ichijo H (2019). Iron homeostasis and iron-regulated ROS in cell death, senescence and human diseases. Biochim Biophys Acta Gen 1863, 1398–1409.

Omary MB, Trowbridge IS (1981). Biosynthesis of the human transferrin receptor in cultured cells. J Biol Chem 256, 12888–12892.
Ponka P, Lok CN (1999). The transferrin receptor: role in health and disease. Int J Biochem Cell Biol 31, 1111–1137.
Recalcati S, Minotti G, Cairo G (2010). Iron regulatory proteins: from molecular mechanisms to drug development. Antioxid Redox Signal 13, 1593–1616.
Robinson MS (2015). Forty years of clathrin-coated vesicles. Traffic 16, 1210–1238.
Rouault TA (2006). The role of iron regulatory proteins in mammalian iron homeostasis and disease. Nat Chem Biol 2, 406–414.
Schwartz AJ, Das NK, Ramakrishnan SK, Jain C, Jurkovic MT, Wu J, Nemeth E, Lakhal-Littleton S, Colacino JA, Shah YM (2019). Hepatic hepcidin/intestinal HIF-2α axis maintains iron absorption during iron deficiency and overload. J Clin Invest 129, 336–348.
Sigismund S, Algisi V, Nappo G, Conte A, Pascolutti R, Cuomo A, Bonaldi T, Argenzio E, Verhoef LG, Maspero E, *et al*. (2013). Threshold-controlled ubiquitination of the EGFR directs receptor fate. EMBO J 32, 2140–2157.
Tachiyama R, Ishikawa D, Matsumoto M, Nakayama KI, Yoshimori T, Yokota S, Himeno M, Tanaka Y, Fujita H (2011). Proteome of ubiquitin/MVB pathway: possible involvement of iron-induced ubiquitylation of transferrin receptor in lysosomal degradation. Genes Cells 16, 448–466.
Thottacherry JJ, Sathe M, Prabhakara C, Mayor S (2019). Spoiled for choice: diverse endocytic pathways function at the cell surface. Annu Rev Cell Dev Biol 35, 55–84.
Truman-Rosentsvit M, Berenbaum D, Spektor L, Cohen LA, Belizowsky-Moshe S, Lifshitz L, Ma J, Li W, Kesselman E, Abutbul-Ionita I, *et al*. (2018). Ferritin is secreted via 2 distinct nonclassical vesicular pathways. Blood 131, 342–352.
Ullrich O, Reinsch S, Urbé S, Zerial M, Parton RG (1996). Rab11 regulates recycling through the pericentriolar recycling endosome. J Cell Biol 135, 913–924.
Vanoaica L, Darshan D, Richman L, Schümann K, Kühn LC (2010). Intestinal ferritin H is required for an accurate control of iron absorption. Cell Metab 12, 273–282.
Young SP, Bomford A, Williams R (1984). The effect of the iron saturation of transferrin on its binding and uptake by rabbit reticulocytes. Biochem J 219, 505–510.